Probabilistic methodology for estimating the optimal photovoltaic capacity in distribution systems to avoid power flow reversals

Juan M. Lujano-Rojas[1,2], Rodolfo Dufo-López[2], José L. Bernal-Agustín[2], José A. Domínguez-Navarro[2], João P. S. Catalão [1,3,4*]

[1] INESC-ID, Instituto Superior Técnico, University of Lisbon, Lisbon 1049-001, Portugal
[2] University of Zaragoza, Zaragoza 50018, Spain
[3] INESC TEC and the Faculty of Engineering of the University of Porto, Porto 4200-465, Portugal
[4] C-MAST, University of Beira Interior, Covilha 6201-001, Portugal
[*]catalao@ubi.pt

Abstract: The large-scale integration of photovoltaic generation (PVG) on distribution systems (DSs) preserving their technical constraints related to voltage fluctuations and active power (AP) flow is a challenging problem. Solar resources are accompanied by uncertainty regarding their estimation and its intrinsically variable nature. This paper presents a new probabilistic methodology based on quasi-static time-series analysis combined with the golden section search algorithm to integrate low and high levels of PVG into DSs to prevent AP flow in reverse direction. Based on the analysis of two illustrative case studies, it was concluded that the successful integration of PVG is not only related to the photovoltaic-cell manufacturing prices and conversion efficiency, but also with the manufacturing prices of power electronic devices required for reactive power control.

1. Nomenclature

d	Index of RP estimation ($d = 1, \dots, J-1$).
h	Index for each hour of the day ($h = 1, \dots, H$)
i	Index for each Monte Carlo trial ($i = 1, \dots, I$).
k	Index for LF calculation ($k = 1, \dots, K$).
m	Index for each month ($m = 1, \dots, M$).
n	Index for each node ($n = 1, \dots, N$).
g	Node at which PVG is installed.
t	Index for hour of the year ($t = 1, \dots, T$).
$\emptyset$	Latitude of the place under analysis (°).
φ	Longitude of the place under analysis (°).
G_t^i	Solar irradiance at time t and trial i (W/m^2).
K_m^i	Clearness index of trail i and month m.
K_m^{min}	Minimum clearness index of month m.
K_m^{max}	Maximum clearness index of month m.
K_m^{nom}	Average clearness index of month m.
T_t	Ambient temperature at time t (°C).
T_m^{min}	Minimum temperature of month m (°C).
T_m^{max}	Maximum temperature of month m (°C).
T_m^{nom}	Nominal temperature of month m (°C).
ρ	Intermediate variable.
ψ_l, χ_l	Variables of temperature model ($l = 1, \dots, 4$).
β	Tilt angle of photovoltaic generator (°).
γ	Azimuth angle of photovoltaic generator (°).
A_{PV}^c	Photovoltaic cell area (cm^2).
N_{PV}	Number of photovoltaic cells on the generator.
FF_{PV}^c	Photovoltaic cell fill factor.
OCV_{PV}^c	Photovoltaic cell open circuit voltage (V).
J_{PV}^c	Photovoltaic cell current density (A/cm^2).
$P_{PV}^{STC,min}$	Minimum PV power to be integrated (kW).
$P_{PV}^{STC,max}$	Maximum PV power to be integrated (kW).
P_{PV}^{STC}	PVG under STC (standard cond.) (kW).
η_{PV}^{STC}	Photovoltaic cell efficiency under STC.
$P_{PV,t}^i$	PVG at time t and trial i (kW).
$\eta_{PV,t}^i$	Cell efficiency at time t and trial i.
α_{PV}^i	Temperature coefficient for trial i (%/°C).
α_{PV}^{min}	Minimum temperature coefficient (%/°C).
α_{PV}^{max}	Maximum temperature coefficient (%/°C).
α_{PV}^{nom}	Nominal temperature coefficient (%/°C).
τ_{PV}^i	PVG de-rating factor for trial i.
τ_{PV}^{min}	Minimum PVG de-rating factor.
τ_{PV}^{max}	Maximum PVG de-rating factor.
τ_{PV}^{nom}	Nominal PVG de-rating factor.
$T_{PV,t}^i$	Cell temperature at time t and trial i (°C).
T_{NOCT}^i	Photovoltaic cell NOCT of trial i (°C).
T_{NOCT}^{min}	Minimum cell NOCT (°C).
T_{NOCT}^{max}	Maximum cell NOCT (°C).
T_{NOCT}^{nom}	Nominal cell NOCT (°C).
P_{PC}	Rated power of converter (kW).
θ, ν, γ	Variables of power converter model.
$\eta_{PC,t}^i$	Power converter efficiency at time t and trial i.
ε	Mean of μ_h series.
θ	Standard deviation of μ_h series.
λ, δ	Parameter of beta PDF.
ω	Autocorrelation of load and price time series.
μ_h	Normalized daily load profile.
σ_h	Uncertainty of normalized daily load profile.
ξ_t^i	White noise value at time t and trial i.
L_t^i	Normalized load (Transformer capacity) and price at time t and trial i.
$\bar{L}_t^i$	Normalized load and price (Gaussian PDF) at time t and trial i.
$\tilde{L}_t^i$	Normalized load and price (Non-Gaussian PDF) at time t and trial i.
$F_L(\cdot)$	CDF of time series $\tilde{L}_t^i$ with $t = 1, \dots, T$ and a determined trail i.
$F_B^{-1}(\cdot)$	Inverse CDF of Beta PDF.
R_n	Resistance of branch n (Ω).
X_n	Reactance of branch n (Ω).
X_{ST}^g	Equivalent reactance at node g (Ω).
F_n	Transformer installed on node n (kVA).
$\overrightarrow{bcbv}$	Row g of BCBV matrix.

$\overrightarrow{bibc}$	Column g of BIBC matrix.
$[BCBV]$	Branch-current to bus-voltage matrix.
$[BIBC]$	Bus-injection to branch-current matrix.
E_{DS}^{max}	Historical peak electricity price (€/kWh).
E_t^i	Energy price at time t and trial i (€/kWh).
V_{DS}^{min}	Minimum voltage of DS (kV).
V_{DS}^{max}	Maximum voltage of DS (kV).
V_{DS}^{nom}	Nominal voltage of DS (kV).
$\vec{V}_{DS}^{min}$	Vector of minimum operational voltage (kV).
$\vec{V}_{DS}^{max}$	Vector of maximum operational voltage (kV).
$\vec{V}_{DS}^{nom}$	Vector of nominal voltage of DS (kV).
S_{DS}^{nom}	Nominal apparent power of DS (kVA).
$S_t^{i,n}$	Load of node n at time t and trial i (kVA).
$P_t^{i,n}$	AP at time t and trial i for node n (kW).
$Q_t^{i,n}$	RP at time t and trial i for node n (kVAr).
Q_{INJ}^{max}	Rated value of RP injected to DS (kVAr).
Q_{CON}^{max}	Rated value of RP consumed from (kVAr).
Q_{STAT}	Rated capacity of STATCOM (kVAr).
$q_{d,t,k}^{i,g}$	RP to be injected/consumed (kVAr).
$\Delta q_{d,t,k}^{i,g}$	Increment of RP (kVAr).
$\Delta q_{d,t,k}^{i,min}$	Minimum increment of RP (kVAr).
$\Delta q_{d,t,k}^{i,max}$	Maximum increment of RP (kVAr).
$I_{t,k}^{i,n}$	Element n of vector $\vec{I}_{t,k}^{i}$ (A).
$V_{t,k}^{i,n}$	Element n of vector $\vec{V}_{t,k}^{i}$ (kV).
$v_{d,t,k}^{i,g}$	Voltage of node g at iteration d (DG model), time t, trial i, and iteration k (LF solution).
$\Delta v_{d,t,k}^{i,g}$	Voltage reduction of node g at iteration d (DG model), time t, trial i, and iteration k (LF solution).
$\vec{I}_{t,k}^{i}$	Vector of current injections at time t and trial i for iteration k (A).
$\vec{V}_{t,k}^{i}$	Vector of voltages at time t and trial i for iteration k (kV).
$\overrightarrow{\Delta V}_{t,k}^{i}$	Vector of voltage reduction at time t and trial i for iteration k (kV).
$\vec{P}_n$	AP of branch n for all trails ($i = 1, \dots, I$) and hours ($t = 1, \dots, T$).
$\vec{Q}_n$	RP of branch n for all trails ($i = 1, \dots, I$) and hours ($t = 1, \dots, T$).
$\vec{I}_n$	Current of branch n for all trails ($i = 1, \dots, I$) and hours ($t = 1, \dots, T$).
$\vec{V}_n$	Voltage of node n for all trails ($i = 1, \dots, I$) and hours ($t = 1, \dots, T$).
ς	Allowed tolerance of LF solution.
$\Delta\varsigma$	Calculation error during LF analysis.
$f_{P,g}(\cdot)$	PDF of AP flow through branch g.
$F_{P,g}^{-1}(\cdot)$	Inverse CDF of AP flow through branch g.
α_{PA}	Significance level for PLF analysis.
α_Q	Significance level for probabilistic RP analysis.
$P_r\{\cdot\}$	Probability of a determined event.
$E\{\cdot\}$	Expected of a probabilistic variable.

2. Introduction

Mass integration of photovoltaic generation (PVG) is currently a crucial and widely analyzed topic due to its importance for the sustainable development of human society. Incorporating renewable energies allows us to reduce our dependence on fossil fuel and consequently the negative impact of human activities on the ecosystem. However, the large-scale integration of PVG faces important problems related to voltage variations and active power (AP) flow in reverse direction, in addition to the increment of short-circuit levels and consequently the degradation of interrupting ratings of circuit breakers and fuses of the distribution system (DS) [1], [2]. Moreover, optimal control of power electronic devices used as interconnection instruments between PVG and DS has been frequently proposed as a strategy to manage voltage fluctuations. However, this option is accompanied by a reduction in power factor, which means a decrement in the AP injected to the DS [3].

Under this panorama, the exhaustive analysis of planning and operation of DS is required. In this sense, many computational tools and design methodologies have been proposed and illustrated in the literature. Computational tools like the Hybrid Optimization Model for Multiple Energy Resources (HOMER), improved Hybrid Optimization by Genetic Algorithms (iHOGA), and Hybrid2 [4] are frequently used to analyze micro-grids, while the integration of PVG and distributed generation (DG) in a determined DS could be analyzed with the Open Distribution System Simulator (OpenDSS) [5] or GridLAB-D [6], among other programs commercially available. On the one hand, HOMER, iHOGA, and Hybrid2 are used to evaluate the performance of a micro-grid under specific environmental conditions without taking into account the impact of DS. However, renewable energy resources can be represented by means of time series in hourly basis. On the other hand, OpenDSS and GridLAB-D are able to perform planning for DSs from a probabilistic perspective, including simulation of annual load and renewable generation. In addition, these tools can also incorporate information from the communication equipment employed by smart-grid infrastructure.

Planning studies for the integration of DG are highly related to the solution of the probabilistic power flow (PPF) problem, which has been addressed in many different manners in the technical literature. Some approaches frequently found are based on the application of Gram-Charlier, Cornish-Fisher, or Edgeworth expansions, the implementation of Monte Carlo simulation (MCS) approach using serial and parallel computing, applying the unscented transformation (UT), among other techniques.

Regarding the application of approximation expansions, the behavior of charging and discharging profiles of electric vehicles (EVs), observed from the perspective of DS, was analyzed in [7] by using a model based on queuing theory combined with a PPF technique. Queuing theory was employed to represent multiple types EVs and plug-in hybrid electric vehicle (PHEVs), while PPF was used to analyze the impact of their charging and discharging profiles on DS. PPF was based on the combination of point estimate and cumulant methods in order to calculate the mean, as well as the high-order characteristics of the voltages and branch powers of DS. In [8], two point estimation method was improved in order to incorporate the correlation level frequently observed among the probabilistic variables that represent renewable power sources. In this way, PPF accuracy can be effectively enhanced. In [9], Gaussian copula theory is used to describe the behavior of non-normal variables, while PPF is transformed to the independent standard normal space. Then, a univariate dimension reduction model combined with two quadrature rules (Gauss-logistic quadrature and Clenshaw-Curtis quadrature) were implemented in order to estimate the moments of the corresponding probabilistic variables obtained from the solution of PPF problem. In [10], the impact of PVG on transmission system was evaluated by means of a PPF model based on cumulants. Specifically, the

Gram-Charlier, Edgeworth, and Cornish-Fisher approximation expansions were considered. Then, a probabilistic model to estimate the probability density function (PDF) of PVG was developed. In [11], the impact of PVG and load demand on transmission system operation was analyzed through the implementation of a PPF based on cumulant method. Applying the Gram-Charlier expansion, PDF of the main probabilistic variables were estimated. Then, a dispatch strategy able to consider the uncertainty related to the PVG was proposed and discussed. In [12], the control of reactive power (RP) on DSs with DG was analyzed. A fast version of PPF, which considers the different sources of uncertainty since their expected values, was used in order to reduce the number of iterations and consequently the computational burden. Then, chaotic particle swarm optimization (PSO) was implemented to determine the optimal setting of generator voltages, transformer taps, and static compensators (STATCOMs), minimizing the real power losses. In [13], the control of carbon emissions was analyzed taking into account the influence of stochastic power generation at regional level. The problem of emissions control was formulated as a multi-objective optimization problem based on PPF analysis, where the correlation of the probabilistic variables was included. The optimization technique is based on the combination of clonal selection algorithm and a fuzzy satisfying decision technique, while PPF is solved by means of Cornish-Fisher expansion.

With respect to the computational implementation of MCS approach to account for the uncertainty related to renewable generation, a mathematical model for sampling of random variables involved in PPF calculations was developed in [14]. The approach is based on the combination of Latin supercube sampling and MCS. In [15], crisscross algorithm is combined with MCS technique to determine the optimal allocation of DG, including the variability in renewable energy generation. In [16], a methodology was developed based on collecting detailed information related to PVG, to be later combined with MCS approach to create a useful benchmark for preliminary estimations of PVG capacity. In [17] was developed a PPF technique that uses a combination of the Johnson system and the improved Sobol's quasi-random number generation approach. Johnson system is used to simulate the PDFs behavior, while Sobol's method is employed to represent the low-discrepancy sample in MCS. In [18], a technique to solve the probabilistic optimal power flow from the evaluation of a PPF was developed. The approach is able to include the correlation of wind speeds using copula theory, while the objectives to be optimized are the expectation and downside risk of fuel cost.

The evolution of computational systems has reduced the time required to solve complex problems in engineering and science. Following these initiative, state-of-the-art computing has been also applied to the planning of DS. In [19], open computing language (OpenCL) was employed as a programming tool for the solution of PPF based on MCS approach. OpenCL was used to take advantage of graphics processing unit (GPU) in order to increase the computational resources available. In [20], GPU has been used to solve PPF based on MCS in a very fast manner, reducing the computational time required to the analysis of a large-scale DS. In [21], a computational tool based on OpenDSS and MATLAB was developed. The computational program is able to perform yearly simulations using parallel computing. In [22], a hybrid simulation tool based on the combination of the electromagnetic transient (EMT) simulation program and OpenDSS has been developed and tested.

As previously mentioned, UT has been also incorporated to the solution of PPF. In [23], a hybrid methodology to solve PPF based on a neural network combined with UT was presented. The methodology takes into account probabilistic and possibilistic information related to DG and PHEV operation, in order to obtain a reliable solution. In [24] was introduced a methodology based on UT, in order to consider several rank-correlated variables with different PDFs. A set of standard Gaussian distributions with Pearson correlation coefficients is created using the Gaussian copula theory. Then, UT is applied to choose the appropriate sample points from Gaussian distributions.

Alternatively, other methodologies have been presented in the literature. In [25], a dimension reduction method to solve PPF is developed and discussed. Considering the independent standard normal space, Nataf transformation was used to evaluate PPF. Then, the generalized lambda PDF is used to represent the sources of uncertainty. In [26], dimension-adaptive sparse grid interpolation (DASGI) was combined with copula theory to efficiently solve PPF. DASGI is particularly useful for high-dimensional probabilistic analysis, while copula theory is used to obtain nonlinear correlation between the different sources of uncertainty. In [27], the stochastic response surface method was employed to solve PPF, in order to avoid using series expansions such as Gram-Charlier, Cornish-Fisher, and Edgeworth. In [28], PPF results were estimated using Parzen window density estimator. Different sources of uncertainty such as wind generation, load demand, and PHEV operation during their connection to DS were considered. The presented method is particularly useful in those cases at which the available information is limited. In [29], it was developed the basis-adaptive sparse polynomial chaos expansion to solve PPF. The method combines the hyperbolic scheme, the least angle regression technique, and the copula theory. As the most important advantage of the presented methodology, it is able to deal with large-scale uncertainty sources and non-linear correlation between them, as well as the reduction on the computational burden. In [30], the influence of tidal power sources on DS was studied by means of a PPF technique based on the implementation of *k*-means clustering algorithm and a non-parametric kernel density estimation approach. The clustering technique aforementioned is used to represent the regularity of the tidal power generation, while the kernel density estimation is used to model its randomness. In [31], probabilistic collocation method was used to represent the correlation of wind speed, and consequently the wind generation, in order to improve the results obtained from PPF. The method processes historical information of wind speed to study the spatial correlation of the power generation observed on neighboring wind farms. In [32], curtailing PVG injection to prevent overvoltage conditions at connection points was proposed; when using this operational strategy, information on solar radiation (SR) for one year is used to determine the proper amount of PVG capacity to be installed, while also taking economic parameters into account. In [33], an analytical model was proposed to determine the integration level of PVG that considers different types of time-varying voltage-dependent load models, using a multi-objective index based on AP and RP losses, as well as voltage fluctuations. In [34], an optimization model based on mixed-integer linear programming (MILP) for planning the integration of wind

energy and PVG was presented. Mathematical models to represent AP and RP flows are linearized, while operational limitations related to voltage fluctuations, feeder ampacities, and substation capacity are included as constraints. Quasi-static time series (QSTS) allows us to incorporate relevant information contained in an historical time series of SR or wind speed, into the planning of DSs. In this sense, the power quality score, which is evaluated through QSTS method, has been introduced in [35] in order to rank the operation of a DS under specific conditions. As QSTS requires a considerable computational effort, a variable-time-step solver was developed in [36] based on backtrack method. Similarly, a technique based on QSTS was developed in [37] able to reduce the computational time spent on the study, implementing accurate mathematical models of control devices of DS.

As can be observed, the study of DS has undergone an important development motivated by the constant growth and adoption of renewable power sources. On the one hand, energy system (ES) analysis requires large amounts of data to be processed, which is related to renewable resources and load demand, typically for one year. On the other hand, the precision of DS analysis and the modeling of its components could impact the process of estimating PVG capacity. These aspects have been considered by combining OpenDSS with EMT or MATLAB and implementing the combination in parallel computational architectures. Besides this, the MILP approach has been suggested; however, the linearization process could influence RP estimation and consequently voltage behavior.

Following the latest trends in DS analysis, in this paper, experience with simulating micro-grids and isolated ESs on a yearly basis is used to study DSs from a probabilistic viewpoint. As a new contribution to earlier studies, QSTS combined with the golden section search algorithm (GSSA) is used in this paper to estimate PVG capacity to be installed in order to avoid reverse AP flow with a determined probability. Low and high penetration levels are considered, depending on the ambition of the system designer; low-penetration PVG systems are connected to DS without any RP support; on the contrary, high-level PVG systems consider the incorporation of RP control to preserve the correct operation of DS. The paper is organized as follows: Section 3 describes the probabilistic model of SR, ambient temperature, load demand, and wholesale prices on a yearly basis; section 4 describes the mathematical model of ES, section 5 explains the proposed methodology, which is described and illustrated in sections 6, 7, and 8. Two DSs of 27 and 84 nodes are studied under low and high integration levels of PVG. The final conclusions are presented in section 9.

3. Renewable Resources, Load Demand, and Electricity Price Simulation

In this section, the probabilistic representation of SR, load, ambient temperature, and wholesale electricity prices by means of MCS is described.

3.1. Solar Resource Simulation

SR is typically evaluated over the long term with the uncertainty considered on annual and hourly basis. From the National Aeronautics and Space Administration (NASA) database, an estimation of the clearness index (CI) including its minimum and maximum value can be obtained. In this paper, this information is used to represent CI by means of triangular PDF, so that those years with high and low potential are modeled by taking their corresponding limits into account, while hourly variability is considered by means of a first-order Markov process, as described by Graham and Hollands in [38]. The process required for generating a set of annual SR time series is briefly described in Algorithm I.

ALGORITHM I
SYNTHETIC GENERATION OF SOLAR RADIATION TIME SERIES

Step 1: Define the location of the PVG system through latitude (ø), longitude (φ), tilt angle (β), and azimuth (γ).

Step 2: Estimate the minimum (K_m^{min}), maximum (K_m^{max}), and average (K_m^{nom}) CI for each month (m) using information taken from the NASA database.

Step 3: Define MCS experiments (I); this is the number of years considered in our analysis. This factor influences the precision at which the uncertainty of SR is modeled.

Step 4: Create a table with T rows and I columns; this table stores each MCS trial required by PPF analysis. As our analysis is carried out on an annual basis, the number of rows is set to T=8760, while I is the number of MCS experiments defined in Step 3.

Step 5: Analyze the first MCS trial by assigning the counter i to 1; or in other words, set i←1.

Step 6: Generate a uniformly random number in the interval [0,1]; then, evaluate this number on each triangular cumulative density function (CDF) defined by the parameters K_m^{min}, K_m^{max}, and K_m^{nom} for each month of the year. From this process, the CI for each month (K_m^i) to be used during this MCS trial (i) is determined.

Step 7: Using the information collected during Steps 1 and 6—specifically, ø, φ, β, γ, and K_m^i, with $m = 1, \dots, M$—evaluate the simulation model proposed by Graham and Hollands [38].

Step 8: Store the SR time series obtained in Step 7 with T elements in the corresponding column (i) of the table previously created in Step 4.

Step 9: If (i<I), then set $i \leftarrow i + 1$ and go to Step 6; else stop.

3.2. Ambient Temperature Simulation

The model presented in [39] could be used to estimate ambient temperature using data from NASA database, as explained in (1) and (2),

$$\rho = 2\pi(h-1)/H\,;\, h = 1, \dots, H; \quad (1)$$

$$T_t = T_m^{nom} + (T_m^{max} - T_m^{min}) \sum_{l=1}^{4} \psi_l cos(l\rho - \chi_l). \quad (2)$$

3.3. Load and Electricity Price Simulation

Using a typical residential load profile (Fig. 1) [40] combined with the capacity of each distribution transformer installed in the DS and the historical peak electricity price

(E_{DS}^{max}), the model described in (3)-(9) and Algorithm II is used to synthetically generate load at each node and an electricity price time series of the wholesale market. Some computational programs such as HOMER [41] use this type of probabilistic model to support the design and optimization of ESs and micro-grids.

$$\bar{L}_t^i = \omega\left(\bar{L}_{t-1}^i\right) + \xi_t^i; t = 1, \dots, T; i = 1, \dots, I; \quad (3)$$
$$\tilde{L}_t^i = \mu_h + \bar{L}_t^i \sigma_h; H = 24; T = 8760;$$

$$h = 1, \dots, H; t = 1, \dots, T; i = 1, \dots, I; \quad (4)$$

$$\lambda = [(1-\varepsilon)\varepsilon^2]/\theta^2 - \varepsilon; \quad (5)$$

$$\delta = [(1-\varepsilon)/\varepsilon]\lambda; \quad (6)$$

$$L_t^i = F_B^{-1}\left(F_L\left(\tilde{L}_t^i\right)\right); t = 1, \dots, T; i = 1, \dots, I; \quad (7)$$

$$S_t^{i,n} = F_n L_t^i;$$

$$n = 1, \dots, N; t = 1, \dots, T; i = 1, \dots, I; \quad (8)$$

$$E_t^i = E_{DS}^{max} L_t^i; t = 1, \dots, T; i = 1, \dots, I. \quad (9)$$

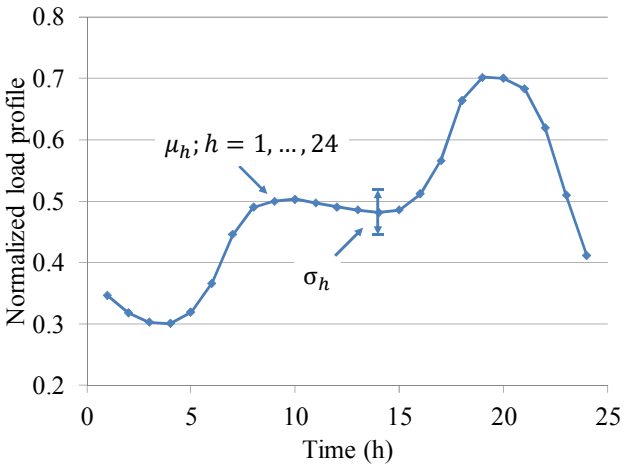

Fig. 1. *Normalized load profile of a typical residential consumer.*

4. Energy System Model

The system under analysis is composed of a PVG system, a power converter, and a DS with or without a distribution STATCOM. The mathematical model of each component is described in the next sub-sections.

4.1. Photovoltaic Generator Model

PVG is represented according to (10)-(13), in which the uncertainty regarding the cell temperature coefficient of power, nominal operating cell temperature (NOCT), and de-rating factor has been introduced using a triangular PDF. This model offers reasonable precision for PVG systems provided with maximum power point tracking [41]:

$$\boldsymbol{T_{PV,t}^i = T_t + \left(\frac{T_{NOCT}^i - 20°C}{800\ W/m^2}\right) G_t^i;} \quad \textbf{(10)}$$

ALGORITHM II
SYNTHETIC GENERATION OF LOAD AND PRICE TIME SERIES

Step 1: Define the number of years under analysis, this is defined by MCS experiments (I).

Step 2: Create a table with T rows and I columns, this table stores each MCS trial required by PPF analysis. As our analysis is carried out annually, the number of rows is set to T=8760 h, while I is the number of MCS experiments (years) defined in Step 1.

Step 3: Analyze the first MCS trial by assigning the counter i to 1. In other words, set i←1.

Step 4: Generate a normalized load and price time series (from a probabilistic perspective) evaluating (3). The result is a vector with T elements and Gaussian PDF.

Step 5: Generate a normalized load and price time series (with respect to the magnitude of loads and prices) evaluating (4), using the results previously obtained in Step 4. The result is a vector with T elements and non-Gaussian PDF.

Step 6: Finally, a normalized load and price time series with respect to the transformer and peak price is obtained by applying the probability transformation of (5)-(7).

Step 7: Estimate the load-demand time series for each node (n) evaluating (8). In a similar way, estimate the electricity price time series by scaling the normalized time series according to (9).

Step 8: Store the load and price time series, obtained in Step 7 with T elements, in the corresponding column (i) of the table previously created in Step 2.

Step 9: If (i<I), then set i←i + 1 and go to Step 4; else stop.

$$\eta_{PV,t}^i = \eta_{PV}^{STC}\left[1 + \alpha_{PV}^i\left(T_{PV,t}^i - 25°C\right)\right]; \quad (11)$$
$$\boldsymbol{P_{PV,t}^i = \left(1 - \tau_{PV}^i\right) A_{PV}^c G_t^i \eta_{PV,t}^i N_{PV};} \quad \textbf{(12)}$$
$$\boldsymbol{P_{PV}^{STC} = FF_{PV}^c OCV_{PV}^c J_{PV}^c A_{PV}^c N_{PV}.} \quad \textbf{(13)}$$

4.2. Power Converter Model

The efficiency of a power converter decreases as the power through it decreases; this phenomenon has been experimentally studied, leading to expression (14) [42]:

$$\eta_{PC,t}^i = \frac{\left(\frac{P_{PV,t}^i}{P_{PC}}\right)}{\left(\frac{P_{PV,t}^i}{P_{PC}} + \theta\right) + \nu\left(\frac{P_{PV,t}^i}{P_{PC}}\right) + \gamma\left(\frac{P_{PV,t}^i}{P_{PC}}\right)^2}. \quad (14)$$

4.3. Distribution System Model

DS has only been modeled for three-phase configurations using the method presented in (15)-(19), implemented according to Algorithm III [43]:

$$S_t^{i,n} = P_t^{i,n} + \left(\sqrt{-1}\right) Q_t^{i,n}; \quad (15)$$

$$I_{t,k}^{i,n} = \left(\frac{S_t^{i,n}}{V_{t,k}^{i,n}}\right)^* ; n = 1, \dots, N \quad (16)$$

$$\vec{I}_{t,k}^{i} = \left[I_{t,k}^{i,1} \quad I_{t,k}^{i,2} \quad \cdots \quad I_{t,k}^{i,N-1} \quad I_{t,k}^{i,N}\right]^T; \quad (17)$$

$$\overrightarrow{\Delta V}_{t,k+1}^{i} = [BCBV][BIBC]\vec{I}_{t,k}^{i}; \quad (18)$$

$$\vec{V}_{t,k+1}^{i} = \vec{V}_{DS}^{nom} - \overrightarrow{\Delta V}_{t,k+1}^{i}; \quad (19)$$

The capacity of STATCOM is determined through the PDF of the RP at the installation point. This PDF is built by using the amount of RP required to maintain the voltage at the installation point at the nominal value (V_{DS}^{nom}). The RP is estimated by following Algorithm IV [44].

5. Proposed Approach

The novel probabilistic methodology proposed in this paper was developed to integrate PVG at low and high levels. Low-level integration assumes that no RP support is installed with the PVG system. Under these circumstances, the flow of AP at installation branch (g) should be moderated to prevent the power from flowing in reverse. The scheme shown in Fig. 2 describes the conditions considered for the incorporation of PVG at low degree. As can be observed, only the local flow of AP is taken into account.

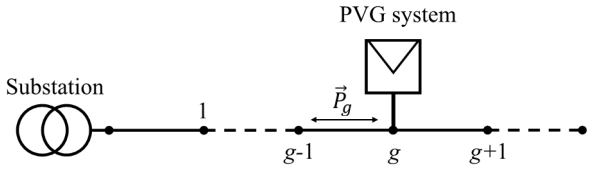

Fig. 2. *Low-level PVG integration architecture.*

Fig. 3 presents the elements considered for the massive incorporation of PVG. In order to preserve the voltage of DS within the acceptable limits, the installation of a distribution STATCOM at the connection point is assumed. On the other hand, high-level penetration is limited by the AP flow at the branch directly connected to the substation ($n = 1$).

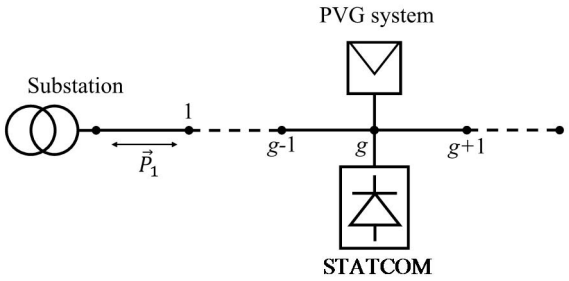

Fig. 3. *High-level PVG integration architecture.*

As stated before, the methodology developed in this work pay special attention to avoid the flow of AP in reverse. Reverse power flow can affect the operation of the energy system as a whole. On the one hand, the inverse power flow can increase the operating costs of the bulk system related to the regulation, ramping generation, and unit commitment. On the other hand, reverse power flow can produce the erratic operation of the protection system, specifically when the reverse power flow is higher than the interruption rating of the corresponding protection device. Similarly, inverse power flow can produce the operation of the reverse power relay installed at the substation, which consequently result in loss of load, degrading the reliability of ES [45].

Fig. 4 illustrates the PDF of AP at the node of interest (g) under very-high and very-low integration of PVG. When the integration level is very low, there is no risk related to the reverse power flow; however, the benefits offered by renewable generation would be very limited. On the contrary, when the integration level is very high, the operational risks related to reverse power flow become considerable. Such risk can be measured by estimating the probability of reverse power flow, shown in shaded region in Fig. 4.

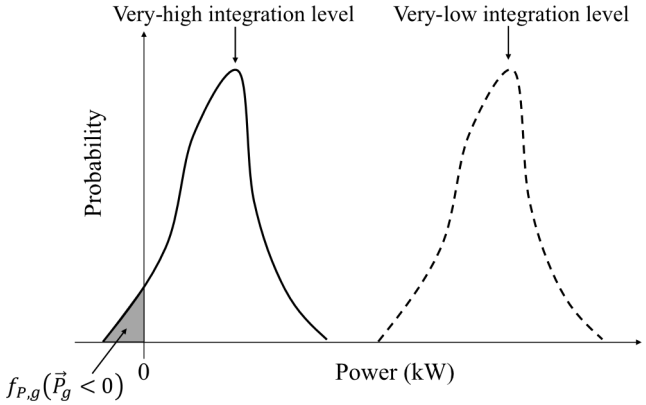

Fig. 4. *Illustration of PDF of AP flow at branch g under very-low and very-high integration level.*

The amount of PVG to be installed could be estimated so that the probability of reverse power flow (shaded region in Fig. 4) is negligible. This idea is mathematically expressed in (31):

$$f_{P,g}(\vec{P}_g < 0) = \alpha_{PA}. \quad (31)$$

At the substation, this reasoning is expressed in (32):

$$f_{P,1}(\vec{P}_1 < 0) = \alpha_{PA}. \quad (32)$$

This idea (equation 32) is the base for the integration of PVG at high-level. PDF of AP flow shown in Fig. 4 can be estimated by means of MCS approach, while the expressions (31) and (32) can be evaluated using linear interpolation. In other words, the method proposed in this paper consists on finding PVG capacity so that the value of $f_{P,g}(\vec{P}_g < 0)$ is equal to the significance level α_{PA}. The factor $f_{P,g}(\vec{P}_g < 0)$ is found by means of the corresponding CDF evaluated at zero through a linear interpolation algorithm.

In this work, the adoption of PVG is made by DS designer. The integration could start with the low-level integration, where a moderated amount of PVG is connected to DS. Then, high-level integration could be performed by increasing the capacity of PVG and by installing an appropriate RP compensation device, a distribution STATCOM.

The next sub-sections clearly describe how is estimated the interval that contains the appropriate PVG capacity to be adopted, how the analysis for the moderated integration of PVG (low-level integration) is performed, and how the study for the massive integration of PVG (high-level integration) is carried out.

5.1. Preliminary PPF Analysis

In order to avoid reverse power flow in a specific branch (g) of DS, power production obtained from PVG system should be equal to the load demanded by DS in that branch. This reasoning can be used to determine the minimum ($P_{PV}^{STC,min}$) and maximum ($P_{PV}^{STC,max}$) PVG capacity that should be considered. The load demanded at the branch under analysis (g) can be probabilistically studied through the solution of PPF problem without considering the influence of any PVG integration. This is known in this paper as the preliminary PPF analysis, which results in the PDF of AP at the branch of interest.

Fig. 5 presents an illustration of the PDF of AP flow at branch g and at the substation (g=1).

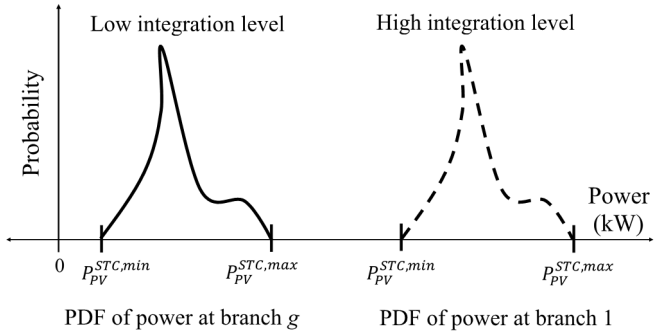

Fig. 5. *Illustration of PDF of AP flow at branch g without any integration of PVG.*

Considering a determined significance level (α_{PA}), the limits for PVG integration can be determined from PDF and CDF of AP flow, as shown in Fig. 5. In summary, a preliminary PPF is performed without considering the AP injection from the PVG system installed at the node of interest. A number of load-demand MCS trials are created to carry out this task, as explained in Algorithm II, and used later in PPF analysis. In case of low-level PVG integration, results obtained from PPF are used to estimate AP flow through branch g ($\vec{P}_g$) and to determine its corresponding PDF ($f_{P,g}$). Similarly, for high-level PVG integration, PPF analysis is used to calculate AP flow from the substation ($\vec{P}_1$) and its PDF ($f_{P,1}$). Then, the required intervals for minimum ($P_{PV}^{STC,min}$) and maximum ($P_{PV}^{STC,max}$) PVG integration, for low and high integration levels, are determined by evaluating the inverse CDF of the AP at branch g ($F_{P,g}^{-1}$) and connected to substation ($F_{P,1}^{-1}$), taking into account the significance level (α_{PA}).

5.2. Low Integration Level of PVG

The proposed method aims to find the rated capacity of PVG system (P_{PV}^{STC}) within the interval $[P_{PV}^{STC,min}, P_{PV}^{STC,max}]$ in order to obtain a probability of reverse power flow $\left(f_{P,g}(\vec{P}_g < 0)\right)$ close to a pre-defined significance level (α_{PA}). This problem can be solved by using GSSA [46] combined with a PPF based on MCS method. GSSA is an iterative optimization method, which requires the evaluation of several points of the interval $[P_{PV}^{STC,min}, P_{PV}^{STC,max}]$ in order to minimize the factor $\left|f_{P,g}(\vec{P}_g < 0) - \alpha_{PA}\right|$. Let us consider the situation at which the performance of a determined PVG capacity (P_{PV}^{STC}) is required to be estimated, this could be understood as the evaluation of a determined iteration of GSSA. To carry out this task, it is necessary to create a specific number (I) of MCS time series of SR using the Algorithm I, as well as load demand and energy prices time series using Algorithm II. The next step consists on performing PPF by solving load flow (LF) problem at each hourly time step ($t = 1, \dots, T$) of each year represented as each MCS trial ($i = 1, \dots, I$). Then, using the results obtained, the PDF ($f_{P,g}$) and consequently the CDF ($F_{P,g}$) of AP flow at the branch of interest (g) is built. At this point, the term $f_{P,g}(\vec{P}_g < 0)$ is calculated through the evaluation of the CDF of AP flow ($F_{P,g}$) at a power equal to zero. Finally, the error is determined by evaluating the factor $\left|f_{P,g}(\vec{P}_g < 0) - \alpha_{PA}\right|$.

As the PVG system is directly connected to DS without any RP support (Fig. 2), PPF can be solved through the application of Algorithm III at each time step and MCS trial.

ALGORITHM III
DISTRIBUTED GENERATION MODELED AS CONSTANT POWER FACTOR

Step 1: Set the tolerance (ς) to a reasonable low value; set the current value of LF calculation error ($\Delta\varsigma$) to an artificially high value ($\Delta\varsigma \leftarrow \infty$); set the current iteration (k) to zero ($k \leftarrow 0$); set the maximum number of iterations (K) to a reasonable value; finally, set the initial value of the vector ($\vec{V}_{t,k}^{i}$) to the nominal system voltage for each node ($\vec{V}_{t,k}^{i} \leftarrow \vec{V}_{DS}^{nom}$). PVG is assumed to be injected on node (g).

Step 2: Using data from the DS, build the matrices $BCBV$ and $BIBC$; useful information can be found in [43].

Step 3: Considering the actual value of vector ($\vec{V}_{t,k}^{i}$), calculate the current injection at each node ($I_{t,k}^{i,n}$; $n = 1, \dots N$) using (15) and (16); in this way, the vector ($\vec{I}_{t,k}^{i}$) defined in (17) is fulfilled.

Step 4: Using the results obtained in steps (2) and (3), estimate the value of vector ($\overrightarrow{\Delta V}_{t,k+1}^{i}$) for the next iteration ($k+1$) using (18).

Step 5: Calculate the value of vector ($\vec{V}_{t,k+1}^{i}$) for the next iteration ($k+1$) using (19).

Step 6: Estimate the current value of the LF calculation error as shown in (20):

$$\Delta\varsigma = \sum_{n=1}^{N} \left| |\vec{V}_{t,k}^{i}| - |\vec{V}_{t,k+1}^{i}| \right|. \quad (20)$$

Step 7: If ($\Delta\varsigma > \varsigma$) and ($k < K$), set $k \leftarrow k+1$ and go to Step 3; else stop.

5.3. High Integration Level of PVG

The study for high penetration of PVG has some similarities to the analysis for the integration at low level. The integration at high level uses the interval obtained from the preliminary analysis described in sub-section 5.1 to determine the rated PVG capacity to be installed, but this process is applied at the branch connected to the substation.

As in the case of low-level integration, GSSA and PPF techniques are combined to estimate the appropriate amount of PVG to be added to DS. However, GSSA is implemented considering the factor $\left|f_{P,1}(\vec{P}_g < 0) - \alpha_{PA}\right|$, while PPF is performed considering the effects of STATCOM installed at the connection point (g). Distribution STATCOM injects or consumes RP in order to maintain the voltage at the connection point at the rating value of the system; this

behavior is included by implementing the Algorithm IV during the solution of PPF. This procedure allows us to obtain the PDF of the RP compensation at the point (g), which provides useful information related to the appropriate capacity of the compensation device to be installed.

Fig. 6 illustrates the PDF of the RP compensation at the node of interest, the magnitudes of RP injected and consumed can be used to estimate the rating capacity of the device to be installed. The quantities of interest in Fig. 6 (Q_{INJ}^{max} and Q_{CON}^{max}) can be calculated by evaluating the corresponding CDF inversely, at a determined significance level (α_Q). Once these variables have been calculated, the capacity of distribution STATCOM (Q_{STAT}) can obtained from the expression $max\{|Q_{INJ}^{max}|, |Q_{CON}^{max}|\}$.

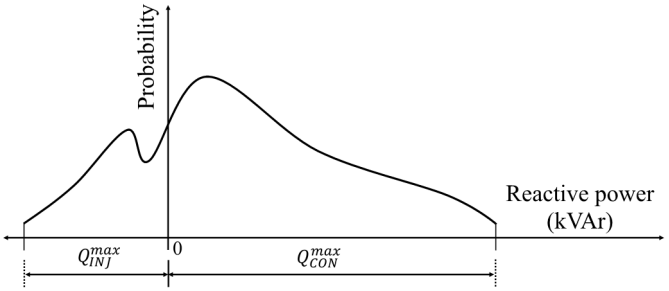

Fig. 6. *Illustration of PDF of required reactive power at node g.*

6. General Conditions of the Case Studies

The technique proposed in this work is illustrated through the study of two hypothetical systems. DS and PVG system are assumed to be located in Zaragoza, Spain ($Ø = 41.65°$ N and $\varphi = 0.833°$ W). Under these conditions, data on SR (K_m^{min}, K_m^{max}, and K_m^{nom}; $m = 1, \dots, M$) and ambient temperature (T_m^{min}, T_m^{max}, and T_m^{nom}) were found on the NASA website on a monthly basis ($M = 12$); the respective models of hourly SR and temperature were later built by following the procedures of sub-sections 3.1 and 3.2.

The load and price time series were synthetically generated according to sub-section 3.3 by considering a peak-price of €0.15/kWh ($E_{DS}^{max} = €0.15/kWh$), and an autocorrelation coefficient of 0.9 ($\omega = 0.9$). Hourly-load uncertainty was modeled as $\sigma_h = 0.15(\mu_h); h = 1, \dots, H$. DS has a rated voltage of 11 kV (V_{DS}^{nom}=11 kV), while its maximum (V_{DS}^{max}) and minimum (V_{DS}^{min}) limits were assumed to be 105% and 95% of the nominal value, respectively.

LF tolerance was adjusted to 0.00001 ($\varsigma = 0.00001$) and the maximum numbers of iterations were adjusted to ($K = 25$) and ($J = 8$).

PVG system was assumed to be installed with a tilt angle of 60º ($\beta = 60°$) and azimuth 0º ($\gamma = 0°$); its production was probabilistically modeled according to sub-section 4.1, assuming NOCT values of $T_{NOCT}^{min} = 45$ °C, $T_{NOCT}^{max} = 48$ °C, and $T_{NOCT}^{nom} = 46°C$; de-rating factors of $\tau_{PV}^{min} = 0.105$, $\tau_{PV}^{max} = 0.42$, and $\tau_{PV}^{nom} = 0.15$; and temperature coefficients of $\alpha_{PV}^{min} = -0.6\ \%/°C$, $\alpha_{PV}^{max} = -0.2\%/°C$, and $\alpha_{PV}^{nom} = -0.5\%/°C$.

GSSA was implemented by assuming $\alpha_{PA} = 0.01$ and $\alpha_Q = 0.01$, while discretized PDFs of AP flow and RP flow were built using 250 intervals. Power converter was modeled by assuming $\theta = 0.0183$, $\nu = 0.0525$, and $\gamma = 0.03768$; the amount of photovoltaic cells (N_{PV}) and rated capacity of power converter (P_{PC}) were adjusted according to the PVG system capacity (P_{PV}^{STC}) under evaluation by the GSSA at each iteration.

ALGORITHM IV
DISTRIBUTED GENERATION MODELED AS CONSTANT VOLTAGE

Step 1: Set the maximum number of iterations (J) to a reasonable value. Considering the node at which DG is installed (g), calculate the corresponding reactance (x_{ST}^g), as shown in (21):

$$x_{ST}^g = img\left(\left[\overrightarrow{bcbv}\right]\left[\overrightarrow{bıbc}\right]\right). \quad (21)$$

Set the initial value ($d = 0$) of RP to be added to DS to zero ($q_{0,t,k}^{i,g} \leftarrow 0$).

Step 2: Set the iteration to one ($d \leftarrow 1$) and voltage to $v_{d,t,k}^{i,g} \leftarrow V_{t,k}^{i,g}$; then, depending on the value of $|v_{d,t,k}^{i,g}|$, determine if it is necessary to inject or consume RP to or from the DS, respectively.

Step 3: If RP needs to be taken from the DS, initialize the range of possible values, as shown in (22):

$$\Delta q_{d,t,k}^{i,g} \in [\Delta q_{d,t,k}^{i,min}, \Delta q_{d,t,k}^{i,max}]; \quad (22)$$

where ($\Delta q_{d,t,k}^{i,min}$) and ($\Delta q_{d,t,k}^{i,max}$) are defined as in (23) and (24), respectively:

$$\Delta q_{d,t,k}^{i,min} = 0; \quad (23)$$

$$\Delta q_{d,t,k}^{i,max} = S_{DS}^{nom}\left(\frac{J-d}{J}\right). \quad (24)$$

Step 4: $\Delta q_{d,t,k}^{i,g}$ is determined by using the GSSA over the interval presented in (23) and (24); the function to be minimized ($\Delta\varsigma$) is built according to (25)-(27) [44]:

$$\Delta v_{d,t,k+1}^{i,g} = X_{ST}^g\left(\frac{\sqrt{-1}\Delta q_{d,t,k}^{i,g}}{v_{d,t,k}^{i,g}}\right)^*; \quad (25)$$

$$v_{d,t,k+1}^{i,g} = V_{DS}^{nom} - \Delta v_{d,t,k+1}^{i,g}; \quad (26)$$

$$\Delta\varsigma = \left(V_{DS}^{nom} - |v_{d,t,k}^{i,g}|\right)^2. \quad (27)$$

Step 5: Once $\Delta q_{d,t,k}^{i,g}$ has been determined to minimize $\Delta\varsigma$, the RP at node g ($q_{d,t,k}^{i,g}$) is computed as in (28):

$$q_{d,t,k}^{i,g} \leftarrow q_{d-1,t,k}^{i,g} + \Delta q_{d,t,k}^{i,g}. \quad (28)$$

If RP needs to be injected to DS, then the corresponding interval of values for ($\Delta q_{d,t,k}^{i,g}$) is defined as in (29) and (30), respectively.

$$\Delta q_{d,t,k}^{i,min} = -S_{DS}^{nom}\left(\frac{J-d}{J}\right); \quad (29)$$

$$\Delta q_{d,t,k}^{i,max} = 0. \quad (30)$$

Then, the estimation error ($\Delta\varsigma$) is minimized as previously explained in (27).

Step 6: Perform a LF calculation according to Algorithm III, considering the value previously defined in (28).

Step 7: If ($d < J - 1$); set $d \leftarrow d + 1$ and go to Step 3; else go to Step 8.

Step 8: Finally, the RP to be injected or consumed at node g is assigned as $Q_{t,k}^i \leftarrow q_{J-1,t,k}^{i,g}$; then, stop.

The photovoltaic cell used in our example was based on Si (Crystalline) technology with $\eta_{PV}^{STC} = 25.6\,\%$, $A_{PV}^{c} = 143.7$ cm^2, $OCV_{PV}^{c} = 0.74$ V, $J_{PV}^{c} = 41.8$ mA/cm^2, and $FF_{PV}^{c} = 82.7\%$ [47].

Additionally, a techno-economic analysis based on net present cost (NPC) estimation is presented by assuming a nominal interest rate of 4%, inflation rate of 2%, project lifetime equal to 45 years, PVG system cost of €1.3/W with lifetime of 30 years, power converter cost of €500/kVA and lifetime of 30 years, and STATCOM capital cost of €50/kVAr with a lifetime of 30 years.

The results obtained from the low and high PVG integration studies are presented in the next sub-sections. The proposed model was implemented in MATLAB on a computer with an i7-3630QM CPU at 2.40 GHz, 8GB of RAM, and a 64-bit operating system.

7. Case A

In this section, the novel probabilistic methodology proposed in this paper for the integration of PVG into a DS is illustrated by analyzing the system shown in Fig. 7 with 27 nodes ($N = 27$) and the parameters presented in Table 1 [48]. As can be observed, PVG is expected to be installed on node 11 ($g = 11$). In this case, load demand time series were created by following the methodology presented in sub-section 3.3 using a general lagging power factor of 0.87.

PPF analysis was performed considering 25 MCS trials (I=25), which means 25 years of SR, ambient temperature, load demand, and energy prices. In addition, a per unit system with base power (S_{DS}^{nom}) of 2100 kVA was used.

The next sub-sections present the results obtained for low and high levels of PVG integration for this case study.

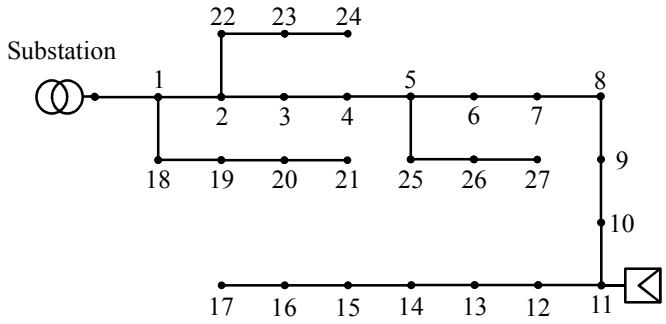

Fig. 7. *Topology of the distribution system under analysis.*

7.1. Results for Low Integration Level (Case A)

GSSA was evaluated to consider PVG capacities between 78.899 kW ($P_{PV}^{STC,min} = 78.899$ kW) and 329.028 kW ($P_{PV}^{STC,max} = 329.028$ kW), according to the results obtained from the preliminary PPF analysis explained in sub-section 5.1. The convergence of GSSA is shown in Fig. 8; this was evaluated through 26 iterations and it suggested the installation of 302 kW, which has a probability of generating reverse power flow in the corresponding branch (g = 11) of 0.011052. Table 2 presents the results of PPF analysis for recommended PVG integration; the reader can observe how the probability of power flowing in reverse slightly increases as a consequence of PVG but with a negligible probability, as $\alpha_{PA} = 0.01$ was chosen. Regarding the techno-economic analysis, the amount of money spent on power purchasing from wholesale market was estimated at €576,920.568/year; while NPC was estimated at €17,879,234.717. The computational time required to design this system was 174.865 minutes.

Additionally, at this integration level the voltages at all nodes were within the required operational limit, or in other words $P_r\{\vec{V}_{DS}^{max} \geq \vec{V}_n \geq \vec{V}_{DS}^{min}\} = \vec{1}$ for $n \in [1,27]$.

7.2. Results for High Integration Level (Case A)

In this case, GSSA was evaluated to consider PVG capacities between 343.911 kW ($P_{PV}^{STC,min} = 343.911$ kW) and 1434.184 kW ($P_{PV}^{STC,max} = 1434.184$ kW), because the main feeder connected to the substation can manage the highest amount of power in DS.

Table 1
Distribution System Information (Case A)

n	R_n (Ω)	X_n (Ω)	F_n (kVA)	Sending Node	Receiving Node
1	0.12648	0.05263	166	Substation	1
2	0.15463	0.06579	94	1	2
3	0.09486	0.03947	100	2	3
4	0.06374	0.02632	117	3	4
5	0.25296	0.10526	94	4	5
6	0.18972	0.07895	98	5	6
7	0.10119	0.04211	98	6	7
8	0.18972	0.07895	94	7	8
9	0.25296	0.10526	103	8	9
10	0.19108	0.05402	94	9	10
11	0.09554	0.02701	-----	10	11
12	0.28663	0.08103	103	11	12
13	0.28663	0.05942	81	12	13
14	0.21019	0.05402	81	13	14
15	0.19108	0.08103	81	14	15
16	0.28663	0.05402	67	15	16
17	0.19108	0.05402	67	16	17
18	0.23886	0.06753	81	1	18
19	0.09554	0.02701	58	18	19
20	0.19108	0.05402	58	19	20
21	0.34395	0.09724	45	20	21
22	0.37339	0.07023	58	2	22
23	0.21019	0.05942	54	22	23
24	0.38217	0.10804	67	23	24
25	0.19108	0.05402	45	5	25
26	0.09554	0.02701	45	25	26
27	0.09554	0.02701	45	26	27

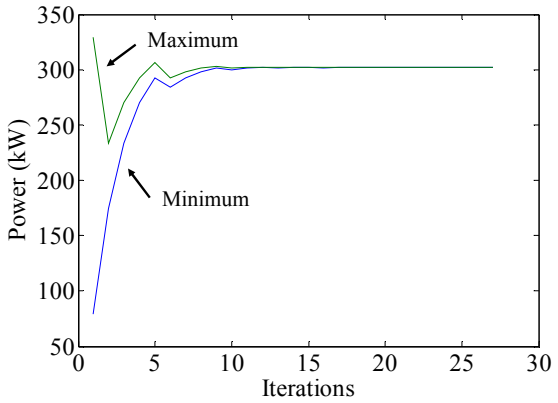

Fig. 8. *Convergence of the GSSA for low-level PVG integration (Case A).*

The convergence of GSSA for this case is shown in Fig. 9. As expected, at 1329 kW the GSSA establishes a probability of producing AP in reverse of 0.010975. It is predicted that €468,391.915/year will be spent on electricity to be imported from the wholesale market, while the expected value of NPC is estimated at €17,308,020.985. The computational time required to design this system was 362.027 minutes. Table 3

presents the averaged performance for this design. It is important to observe how the probability of AP flow in reverse within the DS increases notably, while at the main feeder, this is maintained close to 0.01 according to our design requirements described in (32).

Table 2
Performance of Low-Level PVG Integration (Case A)

n	$E\{\vec{V}_n\}$	$E\{\vec{P}_n\}$	$E\{\vec{Q}_n\}$	$E\{\vec{I}_n\}$	$P_r\{\vec{P}_n < 0\}$
1	10.9878	842.2758	504.9773	51.8276	0
2	10.9759	668.6628	406.5863	41.3513	0
3	10.9699	552.4953	340.7512	34.3378	0
4	10.9662	509.9431	316.6357	31.7695	0
5	10.9527	460.1571	288.4207	28.7653	0
6	10.9447	362.7126	233.1963	22.8859	0
7	10.941	321.0114	209.5632	20.3741	0.0001
8	10.9347	279.3103	185.93	17.8679	0.0001
9	10.9276	239.3112	163.2615	15.4725	0.0004
10	10.9235	195.4824	138.4226	12.8661	0.0019
11	10.9219	155.4834	115.7541	10.5229	0.0111
12	10.9156	204.2505	115.7541	12.4324	0
13	10.9109	160.4218	90.9152	9.7664	0
14	10.9081	125.9545	71.3817	7.6688	0
15	10.9061	91.4872	51.8482	5.5708	0
16	10.9045	57.0199	32.3147	3.4723	0
17	10.9039	28.51	16.1573	1.7362	0
18	10.9852	102.9763	58.3594	6.222	0
19	10.9845	68.509	38.8259	4.1396	0
20	10.9837	43.8288	24.8389	2.6484	0
21	10.983	19.1485	10.8519	1.1571	0
22	10.9731	76.1684	43.1666	4.6077	0
23	10.9719	51.4882	29.1797	3.1149	0
24	10.9708	28.51	16.1573	1.7249	0
25	10.9516	57.4455	32.5558	3.4821	0
26	10.9512	38.297	21.7039	2.3214	0
27	10.951	19.1485	10.8519	1.1607	0

Table 3
Performance of High-Level PVG Integration (Case A)

n	$E\{\vec{V}_n\}$	$E\{\vec{P}_n\}$	$E\{\vec{Q}_n\}$	$E\{\vec{I}_n\}$	$P_r\{\vec{P}_n < 0\}$
1	10.9937	678.28	−365.577	53.9985	0.011
2	10.9892	504.6626	−463.971	49.5578	0.0564
3	10.9876	388.4922	−529.807	47.5539	0.1288
4	10.9869	345.9389	−553.923	47.0663	0.161
5	10.9853	296.1515	−582.139	46.7017	0.1981
6	10.9863	198.7045	−637.365	46.9216	0.2669
7	10.9873	157.0023	−660.999	47.452	0.2932
8	10.9901	115.3001	−684.633	48.16	0.3173
9	10.995	75.3	−707.302	48.9805	0.3397
10	10.9981	31.4701	−732.141	50.0185	0.3649
11	11	−8.5299	−754.81	51.0768	0.3864
12	10.9938	204.2557	115.7571	12.3381	0
13	10.9891	160.4259	90.9175	9.6923	0
14	10.9863	125.9577	71.3835	7.6107	0
15	10.9844	91.4896	51.8495	5.5285	0
16	10.9827	57.0214	32.3155	3.4459	0
17	10.9822	28.5107	16.1578	1.723	0
18	10.9911	102.9789	58.3609	6.2185	0
19	10.9905	68.5108	38.8268	4.1373	0
20	10.9896	43.8299	24.8395	2.647	0
21	10.9889	19.149	10.8522	1.1565	0
22	10.9863	76.1704	43.1677	4.6019	0
23	10.9852	51.4895	29.1804	3.111	0
24	10.984	28.5107	16.1578	1.7227	0
25	10.9842	57.4469	32.5567	3.4712	0
26	10.9838	38.298	21.7044	2.3141	0
27	10.9836	19.149	10.8522	1.1571	0

In order to control the voltage behavior at the installation point (g = 11), the RP requirements are analyzed by means of its PDF, which is shown in Fig. 10. As can be observed, the confidence interval for this distribution has negative and positive values, so that the maximum between the absolute values at extreme points is selected (Fig. 6 in sub-section 5.3), which in our case was 2,349.82 kVAr. At this integration level, the probabilistic condition related to voltage limitations expressed as $P_r\{\vec{V}_{DS}^{max} \geq \vec{V}_n \geq \vec{V}_{DS}^{min}\} = \vec{1}$ for $n \in [1,27]$ is also fulfilled.

When comparing the low- and high-integration models, a difference of 18.8% in the costs related to the energy imported from wholesale market is observed. However, a modest difference of NPC by only 3.2% is estimated. Based on these results, it is possible to conclude that the economic success of PVG integration at a high level not only depends on the increment of photovoltaic-cell efficiency and the reduction of its manufacturing costs but also on the costs related to the power electronic devices required to support and improve the voltage profile.

Another relevant result is the difference in the computational times required to analyze low and high integration levels.

As stated before in Algorithm IV, an additional procedure to determine the RP to be injected or consumed in order to maintain the voltage at the installation point at its nominal value is required; this process is carried out in a loop $J-1$ times, incrementing the computational burden of the mathematical problem.

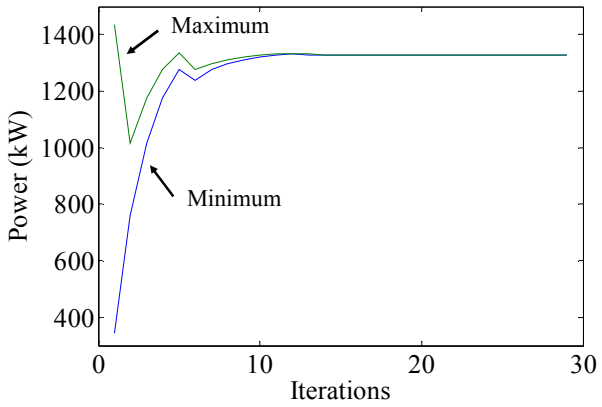

Fig. 9. *Convergence of the GSSA for high-level PVG integration (Case A).*

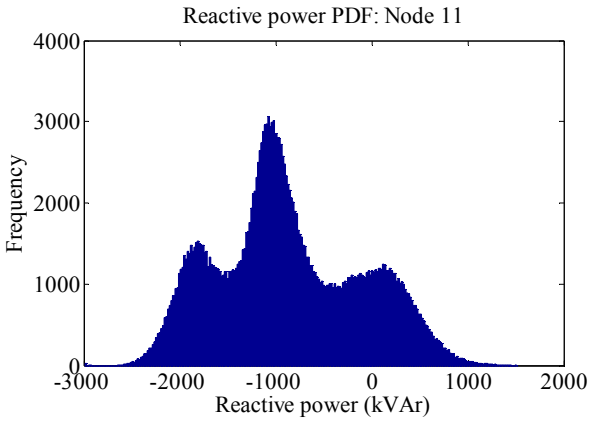

Fig. 10. *PDF of required reactive power (Case A).*

8. Case B

The proposed methodology is illustrated through the analysis of another DS of 84 nodes ($N = 84$). The parameters of the system are shown in Table 4 [49]. PVG system is supposed to be installed on node 26 ($g = 26$). As in the previous case, load demand time series were created by following the methodology presented in sub-section 3.3 using a general lagging power factor of 0.9.

PPF analysis was performed considering 5 MCS trials (I=5), and using a per unit system with base power (S_{DS}^{nom}) of 3000 kVA. The next sub-sections present the results obtained for low and high levels of PVG integration for this case.

8.1. Results for Low Integration Level (Case B)

From the implementation of the preliminary PPF analysis explained in sub-section 5.1 for this case study, PVG capacity considered during the evaluation of GSSA is between 129.863 kW ($P_{PV}^{STC,min} = 129.863$ kW) and 541.558 kW ($P_{PV}^{STC,max} = 541.558$ kW). The convergence of GSSA is shown in Fig. 11, which suggests the installation of a PVG system of 488 kW. The probability of reverse power flow at the branch 26 (g=26) is 0.007841, these results can be verified in the averaged performance presented in Table 5. As in our previous case study, the probability of observing reverse power flow rapidly decreases, for those branches towards the main substation. Moreover, the amount of money spent on power purchasing from wholesale market was estimated at €720,692.751/year; while NPC was estimated in €22,603,477.236. The computational time required to design this system was 125.101 minutes.

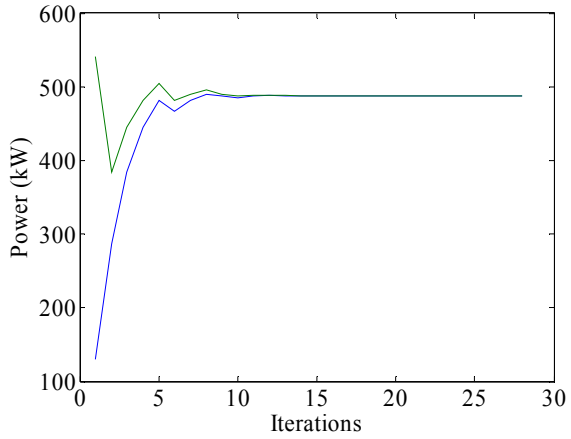

Fig. 11. *Convergence of the GSSA for low-level PVG integration (Case B).*

Using the information obtained from the preliminary PPF study, GSSA was evaluated to consider PVG capacities between 435.457 kW ($P_{PV}^{STC,min}$ = kW) and 1815.951 kW ($P_{PV}^{STC,max}$ = kW), because the main feeder connected to the substation can manage the highest amount of power in the DS. The convergence of GSSA for this analysis is shown in Fig. 12 suggesting the installation of a PVG system of 1704 kW. As can be observed in Table 6, at 1704 kW the probability of producing AP in reverse flow at the substation is 0.011559.

It is expected that €589,869.581/year will be spent on electricity to be imported from the wholesale market, while the expected value of NPC is estimated in €21,870,226.668. The computational time required to design this system was 313.112 minutes.

Table 4
Distribution System Information (Case B)

n	R_n (Ω)	X_n (Ω)	F_n (kVA)	Sending Node	Receiving Node
1	0.108	0.075	0	Substation	1
2	0.163	0.112	0	1	2
3	0.217	0.149	56	2	3
4	0.108	0.074	0	3	4
5	0.435	0.298	35	4	5
6	0.272	0.186	0	5	6
7	1.197	0.82	35	6	7
8	0.108	0.074	0	7	8
9	0.598	0.41	0	8	9
10	0.544	0.373	56	9	10
11	0.544	0.373	0	10	11
12	0.598	0.41	0	11	12
13	0.272	0.186	35	12	13
14	0.326	0.223	35	13	14
15	0.728	0.302	35	1	15
16	0.455	0.189	112	2	16
17	0.82	0.34	56	4	17
18	0.637	0.264	56	17	18
19	0.455	0.189	35	18	19
20	0.819	0.34	35	19	20
21	1.548	0.642	35	20	21
22	0.182	0.075	56	18	22
23	0.91	0.378	35	6	23
24	0.455	0.189	35	7	24
25	0.364	0.151	56	24	25
26	0.546	0.226	-----	25	26
27	0.273	0.113	56	26	27
28	0.546	0.226	0	27	28
29	0.546	0.226	35	28	29
30	0.273	0.113	35	29	30
31	0.182	0.075	0	30	31
32	0.182	0.075	14	31	32
33	0.819	0.34	0	32	33
34	0.637	0.264	0	33	34
35	0.182	0.075	35	34	35
36	0.364	0.151	56	25	36
37	1.002	0.416	56	26	37
38	0.546	0.226	56	28	38
39	0.455	0.189	35	31	39
40	1.002	0.416	0	39	40
41	0.273	0.113	35	40	41
42	0.455	0.189	35	40	42
43	1.002	0.416	35	33	43
44	0.911	0.378	35	43	44
45	0.911	0.378	35	44	45
46	0.546	0.226	14	45	46
47	0.637	0.264	0	34	47
48	0.182	0.075	0	47	48
49	0.364	0.151	36	48	49
50	0.455	0.189	56	49	50
51	1.366	0.567	0	47	51
52	0.455	0.189	35	51	52
53	0.546	0.226	56	52	53
54	0.546	0.226	56	51	54
55	0.546	0.226	14	48	55
56	0.273	0.113	56	8	56
57	0.819	0.34	0	56	57
58	0.182	0.075	56	57	58
59	0.546	0.226	56	57	59
60	0.728	0.302	56	59	60
61	1.002	0.415	56	60	61
62	0.182	0.075	14	59	62
63	0.728	0.302	0	62	63
64	0.182	0.075	0	63	64
65	0.182	0.075	56	64	65
66	0.455	0.189	0	63	66
67	0.91	0.378	0	66	67
68	1.092	0.453	56	67	68
69	0.455	0.189	0	68	69
70	0.546	0.226	35	69	70
71	0.182	0.075	56	66	71
72	1.184	0.491	0	67	72
73	0.273	0.113	56	72	73
74	1.002	0.416	35	72	74
75	0.546	0.226	56	69	75
76	0.091	0.037	14	64	76
77	0.637	0.264	56	9	77
78	0.546	0.226	35	66	78
79	0.728	0.302	56	11	79
80	0.364	0.151	0	79	80
81	0.091	0.037	56	80	81
82	1.092	0.453	35	80	82
83	1.002	0.416	14	82	83
84	0.819	0.34	35	12	84

In order to control the voltage behavior at the installation point (g = 26), the RP requirements are analyzed by means of its PDF, which is shown in Fig. 13. As can be observed, the confidence interval for this distribution has negative and positive values, so that the maximum between the absolute values at extreme points is selected (Fig. 6 in sub-section 5.3), which in this case was 2963.02 kVAr.

8.2. Results for High Integration Level (Case B)

With respect to the difference of NPC and annual costs of energy purchase, similar results to those obtained in Case A can be found, which reveals the importance of power electronic devices on the economic sustainability of PVG integration. On the one hand, the rated capacity of distribution STATCOM is similar in both case studies, specifically at high level integration.

Table 5
Performance of Low-Level PV Integration (Case B)

n	$E\{\vec{V}_n\}$	$E\{\vec{P}_n\}$	$E\{\vec{Q}_n\}$	$E\{\vec{I}_n\}$	$P_r\{\vec{P}_n < 0\}$
1	10.9855	1051.467	546.4821	64.1193	0
2	10.964	1036.058	539.0194	63.2206	0
3	10.9367	986.7508	515.1388	60.3385	0
4	10.9235	962.0971	503.1985	58.8941	0
5	10.8765	841.9106	444.9895	51.8333	0
6	10.8477	826.5021	437.5269	50.9258	0
7	10.7229	811.0936	430.0642	50.0157	0
8	10.7166	471.5009	228.3583	28.4348	0
9	10.7041	166.4121	80.5971	10.0115	0
10	10.6945	141.7584	68.6567	8.5308	0
11	10.6865	117.1048	56.7164	7.049	0
12	10.6831	46.2256	22.3881	2.782	0
13	10.682	30.8171	14.9254	1.8546	0
14	10.6814	15.4085	7.4627	0.9274	0
15	10.9843	15.4085	7.4627	0.9	0
16	10.9616	49.3073	23.8806	2.8863	0
17	10.9126	120.1865	58.209	7.0741	0
18	10.9059	95.5329	46.2687	5.6241	0
19	10.9036	46.2256	22.3881	2.722	0
20	10.9008	30.8171	14.9254	1.8149	0
21	10.8982	15.4085	7.4627	0.9076	0
22	10.9054	24.6536	11.9403	1.4511	0
23	10.8461	15.4085	7.4627	0.9122	0
24	10.7055	324.1841	194.2432	20.8754	0.0015
25	10.6922	308.7756	186.7805	19.9731	0.0022
26	10.6753	259.4683	162.8999	17.1073	0.0078
27	10.6656	311.6925	150.9596	18.9114	0
28	10.6478	287.0388	139.0193	17.4252	0
29	10.6315	262.3852	127.079	15.9361	0
30	10.6239	246.9767	119.6163	15.0041	0
31	10.6191	231.5681	112.1536	14.0713	0
32	10.6152	185.3426	89.7655	11.2701	0
33	10.5985	179.1792	86.7804	10.8967	0
34	10.5893	126.7902	61.4073	7.7139	0
35	10.589	15.4085	7.4627	0.9361	0
36	10.6912	24.6536	11.9403	1.4823	0
37	10.6725	24.6536	11.9403	1.4852	0
38	10.6463	24.6536	11.9403	1.4891	0
39	10.6167	46.2256	22.3881	2.8012	0
40	10.6132	30.8171	14.9254	1.8677	0
41	10.6127	15.4085	7.4627	0.9338	0
42	10.6124	15.4085	7.4627	0.9339	0
43	10.5926	52.389	25.3731	3.1827	0
44	10.5887	36.9805	17.9105	2.247	0
45	10.5865	21.5719	10.4478	1.3109	0
46	10.5861	6.1634	2.9851	0.3745	0
47	10.5813	111.3816	53.9446	6.7778	0
48	10.5803	46.6658	22.6013	2.8382	0
49	10.5786	40.5024	19.6162	2.4634	0
50	10.5773	24.6536	11.9403	1.4995	0
51	10.5712	64.7158	31.3433	3.9397	0
52	10.5691	40.0622	19.403	2.439	0
53	10.5676	24.6536	11.9403	1.501	0
54	10.5696	24.6536	11.9403	1.5007	0
55	10.5799	6.1634	2.9851	0.3748	0
56	10.7072	305.0888	147.7613	18.4234	0
57	10.6812	280.4352	135.821	16.9434	0
58	10.6807	24.6536	11.9403	1.4839	0
59	10.6654	255.7815	123.8807	15.4596	0
60	10.6613	49.3073	23.8806	2.9739	0
61	10.6585	24.6536	11.9403	1.4872	0
62	10.6616	181.8206	88.0597	10.9995	0
63	10.6471	175.6572	85.0747	10.6278	0
64	10.6465	30.8171	14.9254	1.8613	0
65	10.646	24.6536	11.9403	1.4891	0
66	10.6397	144.8402	70.1493	8.7665	0
67	10.6289	104.778	50.7463	6.345	0
68	10.6209	64.7158	31.3433	3.9195	0
69	10.6188	40.0622	19.403	2.4267	0
70	10.6178	15.4085	7.4627	0.9333	0
71	10.6392	24.6536	11.9403	1.4901	0
72	10.6235	40.0622	19.403	2.4255	0
73	10.6227	24.6536	11.9403	1.4926	0
74	10.6217	15.4085	7.4627	0.9329	0
75	10.6173	24.6536	11.9403	1.4934	0
76	10.6464	6.1634	2.9851	0.3722	0
77	10.7024	24.6536	11.9403	1.4806	0
78	10.6387	15.4085	7.4627	0.9313	0
79	10.6807	70.8792	34.3284	4.267	0
80	10.6788	46.2256	22.3881	2.7832	0
81	10.6786	24.6536	11.9403	1.4842	0
82	10.6762	21.5719	10.4478	1.299	0
83	10.6755	6.1634	2.9851	0.3712	0
84	10.6817	15.4085	7.4627	0.9273	0

Table 6
Performance of High-Level PV Integration (Case B)

n	$E\{\vec{V}_n\}$	$E\{\vec{P}_n\}$	$E\{\vec{Q}_n\}$	$E\{\vec{I}_n\}$	$P_r\{\vec{P}_n < 0\}$
1	10.9956	854.2241	-704.335	64.8441	0.0116
2	10.9892	838.8179	-711.797	64.383	0.0132
3	10.982	789.5179	-735.674	62.9714	0.0203
4	10.9788	764.8679	-747.612	62.3051	0.0247
5	10.9725	644.6993	-805.813	59.4651	0.0585
6	10.9692	629.293	-813.274	59.1622	0.0639
7	10.9586	613.8868	-820.736	58.877	0.0703
8	10.9524	471.4309	228.3244	27.7662	0
9	10.9402	166.3874	80.5851	9.7773	0
10	10.9308	141.7374	68.6466	8.3311	0
11	10.9231	117.0874	56.708	6.8839	0
12	10.9197	46.2187	22.3847	2.7168	0
13	10.9187	30.8125	14.9232	1.8112	0
14	10.918	15.4062	7.4616	0.9056	0
15	10.9944	15.4062	7.4616	0.899	0
16	10.9867	49.3	23.8771	2.8788	0
17	10.968	120.1687	58.2003	7.0348	0
18	10.9614	95.5187	46.2618	5.5928	0
19	10.9591	46.2187	22.3847	2.7068	0
20	10.9563	30.8125	14.9232	1.8048	0
21	10.9537	15.4062	7.4616	0.9025	0
22	10.9609	24.65	11.9385	1.443	0
23	10.9676	15.4062	7.4616	0.9013	0
24	10.9706	127.0496	-1056.52	61.8942	0.3266
25	10.9811	111.6434	-1063.98	62.2556	0.333
26	11	62.3434	-1087.86	63.4846	0.3549
27	10.9906	311.6462	150.9372	18.3009	0
28	10.9734	286.9962	138.9986	16.862	0
29	10.9576	262.3463	127.0601	15.4206	0
30	10.9502	246.94	119.5985	14.5184	0
31	10.9456	231.5338	112.1369	13.6156	0
32	10.9419	185.3151	89.7522	10.9046	0
33	10.9257	179.1526	86.7675	10.5432	0
34	10.9168	126.7713	61.3982	7.4635	0
35	10.9165	15.4062	7.4616	0.9058	0
36	10.9801	24.65	11.9385	1.4403	0
37	10.9973	24.65	11.9385	1.4379	0
38	10.9719	24.65	11.9385	1.4415	0
39	10.9433	46.2187	22.3847	2.711	0
40	10.9399	30.8125	14.9232	1.8076	0
41	10.9394	15.4062	7.4616	0.9038	0
42	10.9391	15.4062	7.4616	0.9038	0
43	10.9199	52.3812	25.3694	3.0797	0
44	10.9162	36.975	17.9078	2.1742	0
45	10.914	21.5687	10.4462	1.2684	0
46	10.9137	6.1625	2.9846	0.3624	0
47	10.909	111.3651	53.9366	6.5577	0
48	10.908	46.6589	22.5979	2.7461	0
49	10.9064	40.4964	19.6133	2.3834	0
50	10.9052	24.65	11.9385	1.4509	0
51	10.8992	64.7062	31.3386	3.8116	0
52	10.8972	40.0562	19.4001	2.3597	0
53	10.8957	24.65	11.9385	1.4522	0
54	10.8977	24.65	11.9385	1.4519	0
55	10.9077	6.1625	2.9846	0.3626	0
56	10.9432	305.0435	147.7393	17.9889	0
57	10.9178	280.3936	135.8008	16.5435	0
58	10.9173	24.65	11.9385	1.4491	0
59	10.9024	255.7436	123.8623	15.0943	0
60	10.8984	49.3	23.8771	2.904	0
61	10.8957	24.65	11.9385	1.4522	0
62	10.8987	181.7936	88.0467	10.7391	0
63	10.8846	175.6311	85.062	10.3762	0
64	10.884	30.8125	14.9232	1.8174	0
65	10.8835	24.65	11.9385	1.4539	0
66	10.8773	144.8187	70.1389	8.5588	0
67	10.8668	104.7624	50.7388	6.1945	0
68	10.8589	64.7062	31.3386	3.8265	0
69	10.8569	40.0562	19.4001	2.3691	0
70	10.856	15.4062	7.4616	0.9112	0
71	10.8768	24.65	11.9385	1.4549	0
72	10.8615	40.0562	19.4001	2.368	0
73	10.8608	24.65	11.9385	1.4572	0
74	10.8598	15.4062	7.4616	0.9108	0
75	10.8554	24.65	11.9385	1.4579	0
76	10.8839	6.1625	2.9846	0.3635	0
77	10.9385	24.65	11.9385	1.4461	0
78	10.8764	15.4062	7.4616	0.9093	0
79	10.9174	70.8687	34.3233	4.1671	0
80	10.9155	46.2187	22.3847	2.718	0
81	10.9153	24.65	11.9385	1.4494	0
82	10.9129	21.5687	10.4462	1.2686	0
83	10.9123	6.1625	2.9846	0.3625	0
84	10.9183	15.4062	7.4616	0.9056	0

For Case A, a device of 2,349.82 kVAr was suggested, while for Case B the capacity found was 2963.02 kVAr. From Figs. 10 and 13, it is possible to observe that these values are directly related to the injection of RP, which highly depends on the load profile of Fig. 1. On the other hand, incorporation of RP compensation device is not so evident in Case A, where the voltage at all nodes is within the required interval. However, in Case B this does not occur.

Table 7 shows the probabilistic analysis of voltage at each node for both integration levels, at low-level integration there is a low probability of observing voltage variations out the required limits because there is no any RP control. On the contrary, incorporation of distribution STATCOM in the high-level option guarantee proper magnitudes of the voltage at each node.

Another important topic is the effect of the number of MCS trials on the PVG capacity estimation and performance. In Case B only were considered 5 years (I=5) in order to reduce the computational time. However, the precision of method could be improved by incrementing the number of experiments, spending more computational time. Table 8 presents the value of some parameters such as PVG capacity, STATCOM capacity, probability of reverse power flow, expected value of NPC, and computational time when 10 years are considered on MCS method (I=10). As can be concluded, for this specific case, the results obtained for 10 MCS trials are very similar to those previously reported.

Table 7
Values of $P_r\{\vec{V}_{DS}^{max} \geq \vec{V}_n \geq \vec{V}_{DS}^{min}\}$ for Case B

n	Low-Level PVG	High-Level PVG
1	1	1
2	1	1
3	1	1
4	1	1
5	1	1
6	1	1
7	0.9999	1
8	0.9997	1
9	0.9988	1
10	0.9973	1
11	0.9951	1
12	0.994	1
13	0.9934	1
14	0.9931	1
15	1	1
16	1	1
17	1	1
18	1	1
19	1	1
20	1	1
21	1	1
22	1	1
23	1	1
24	0.9986	1
25	0.9951	1
26	0.9842	1
27	0.9753	1
28	0.9539	1
29	0.9274	1
30	0.9128	1
31	0.9038	1
32	0.8962	1
33	0.864	1
34	0.8463	1
35	0.8458	1
36	0.9947	1
37	0.9816	1
38	0.9517	1
39	0.8989	1
40	0.8922	1
41	0.8914	1
42	0.8908	1
43	0.8523	1
44	0.8453	1
45	0.8413	1
46	0.8407	1
47	0.8321	1
48	0.8303	1
49	0.8273	1
50	0.8251	1
51	0.8154	1
52	0.8118	1
53	0.8089	1
54	0.8128	1
55	0.8296	1
56	0.9992	1
57	0.9929	1
58	0.9927	1
59	0.9839	1
60	0.9803	1
61	0.9778	1
62	0.9806	1
63	0.9656	1
64	0.9648	1
65	0.9641	1
66	0.9559	1
67	0.9392	1
68	0.925	1
69	0.9208	1
70	0.9189	1
71	0.9552	1
72	0.9295	1
73	0.9281	1
74	0.9265	1
75	0.9178	1
76	0.9647	1
77	0.9986	1
78	0.9545	1
79	0.9927	1
80	0.9919	1
81	0.9918	1
82	0.9908	1
83	0.9904	1
84	0.9932	1

Table 8
Brief results considering 10 MCS trials

Parameters	Low-Level Integration	High-Level Integration
P_{PV}^{STC} (kW)	498	1673
Q_{STAT} (kVAr)	-----	2,959.68
$P_r\{\vec{P}_n < 0\}$	0.008813	0.010123
$E\{NPC\}$ (€)	22,602,936.33	21,867,782
Time (minutes)	245.66975	601.773167

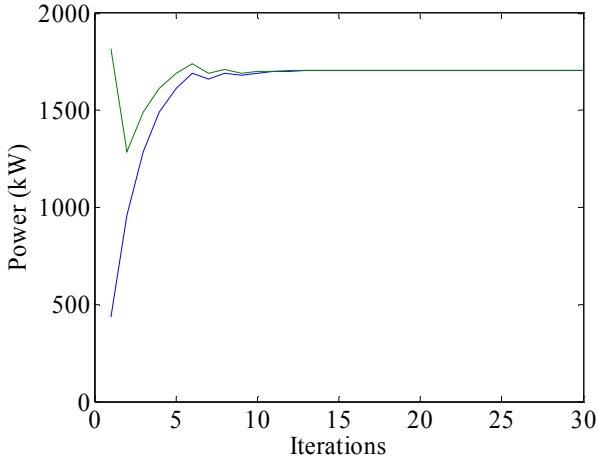

Fig. 12. *Convergence of the GSSA for high-level PVG integration (Case B).*

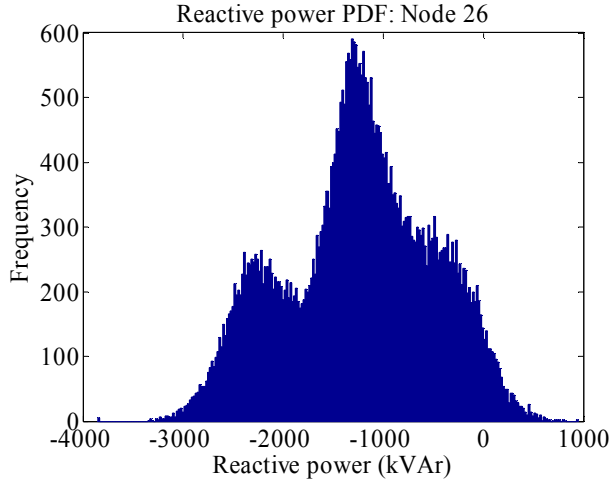

Fig. 13. *PDF of required reactive power (Case B).*

9. Conclusions

In this paper, GSSA was combined with QSTS analysis as a new contribution to determine the proper amount of PVG needed to prevent AP flow in reverse. The novel probabilistic methodology could be implemented in two different stages: at a low level of integration, installing PVG at a moderated rate, and at a high level, by incrementing PVG at a massive rate accompanied with a distribution STATCOM device to guarantee optimal behavior of the voltage profile. The analysis of two illustrative case studies allowed concluding that the economic viability of massive PVG incorporation requires a considerable increase in cell efficiencies as well as decreased cell and STATCOM manufacturing costs and prices, which are required to operationally support high-level integration. Otherwise, the feeders' ampacity was not included in the proposed methodology study. However, if the probability of overload for a determined feeder n is higher than α_{PA}, then the proposed algorithm could be applied again, assigning the low limit of the GSSA searching interval ($P_{PV}^{STC,min}$) to that obtained from the preliminary PPF and high limit of the GSSA searching interval for the PVG capacity that was recently found ($P_{PV}^{STC,max} \leftarrow P_{PV}^{STC}$). In this way, the probability of reverse AP flow will be lower than α_{PA}, while the probability of overloading any feeder can be adjusted to a value close to α_{PA}. A similar reasoning can be applied to reduce the probability of over-voltage or under-voltage in any node of the DS.

The proposed methodology has very theoretical characteristics. However, it could be used to approximate the photovoltaic generation capacity from general information of the system of interest. For example, the load profile of Fig. 1 could be measured by means of a three-phase power logger installed at the substation. On the other hand, the implementation of the low-level integration and then the high-penetration design allows DS operator to overcome any technical issue, since the integration process starts by the minimum impact configuration, gradually.

10. Acknowledgments

This work was supported by FEDER funds through COMPETE 2020 and by Portuguese funds through FCT, under Projects SAICT-PAC/0004/2015 - POCI-01-0145-FEDER-016434, POCI-01-0145-FEDER-006961, UID/EEA/50014/2013, UID/CEC/50021/2013, UID/EMS/00151/2013, SFRH/BPD/103079/2014, and 02/SAICT/2017 - POCI-01-0145-FEDER-029803. Also, the research leading to these results has received funding from the EU Seventh Framework Programme FP7/2007-2013 under grant agreement no. 309048. Moreover, this work was supported by the Ministerio de Economía y Competitividad of the Spanish Government under Project ENE2013-48517-C2-1-R.

11. References

[1] Petinrin, J. O., Shaaban, M.: 'Impact of renewable generation on voltage control in distribution systems', *Renew. Sust. Energ. Rev.*, 2016, 65, pp. 770-783

[2] Yang, Y., Enjeti, P., Blaabjerg, F., Wang, H.: 'Wide-scale adoption of photovoltaic energy: Grid code modifications are explored in the distribution grid', *IEEE Ind. Appl. Mag.*, 2015, 21, (5), pp. 21-31

[3] Liu, E., Bebic, J.: 'Distribution system voltage performance analysis for high-penetration photovoltaics'. *National Renewable Energy Laboratory*, Golden, CO, Tech. rep. NREL/SR-581-42298, February 2008

[4] Sinha, S., Chandel, S. S.: 'Review of software tools for hybrid renewable energy systems', *Renew. Sust. Energ. Rev.*, 2014, 32, pp. 192-205

[5] Dugan, R. C.: 'The open distribution system simulator (OpenDSS)'. *Electric Power Research Institute*, Palo Alto, CA, March 2016

[6] Martinez, J. A., Dinavahi, V., Nehrir, M. H., Guillaud, X.: 'Tools for analysis and design of distributed resources-Part IV: Future trends', *IEEE Trans. Power Del.*, 2011, 26, (3), pp. 1671-1680

[7] Li, G., Zhang, X.-P.: 'Modeling of plug-in hybrid electric vehicle charging demand in probabilistic power flow calculations', *IEEE Trans. Smart Grid*, 2012, 3, (1), pp. 492-499

[8] Aien, M., Khajeh, M. G., Rashidinejad, M., Fotuhi-Firuzabad, M.: 'Probabilistic power flow of correlated hybrid wind-photovoltaic power systems', *IET Renew. Power Gener.*, 2014, 8, (6), pp. 649-658

[9] Xiao, Q., He, Y., Chen, K., Yang, Y., Lu, Y.: 'Point estimate method based on univariate dimension reduction model for probabilistic power flow computation', *IET Gener. Transm. Distrib.*, 2017, 11, (14), pp. 3522-3531

[10] Fan, M., Vittal, V., Heydt, G. T., Ayyanar, R.: 'Probabilistic power flow studies for transmission systems with photovoltaic generation using cumulants', *IEEE Trans. Power Syst.*, 2012, 27, (4), pp. 2251-2261

[11] Fan, M., Vittal, V., Heydt, G. T., Ayyanar, R.: 'Probabilistic power flow analysis with generation dispatch including photovoltaic resources', *IEEE Trans. Power Syst.*, 2013, 28, (2), pp. 1797-1805

[12] Hong, Y.-Y., Lin, F.-J., Lin, Y.-C., Hsu, F.-Y.: 'Chaotic PSO-based VAR control considering renewables using fast probabilistic power flow', *IEEE Trans. Power Del.*, 2014, 29, (4), pp. 1666-1674

[13] Wang, X., Gong, Y., Jiang, C.: 'Regional carbon emission management based on probabilistic power flow with correlated stochastic variables', *IEEE Trans. Power Syst.*, 2015, 30, (2), pp. 1094-1103

[14] Hajian, M., Rosehart W. D., Zreipour, H.: 'Probabilistic power flow by Monte Carlo simulation with Latin supercube sampling', *IEEE Trans. Power Syst.*, 2013, 28, (2), pp. 1550-1559

[15] Peng, X., Lin, L., Zheng, W., Liu, Y.: 'Crisscross optimization algorithm and Monte Carlo Simulation for solving optimal distributed generation allocation problem', *Energies*, 2015, 8, (12), pp. 13641-13659

[16] Navarro-Espinosa, A., Ochoa, L. F.: 'Probabilistic impact assessment of low carbon technologies in LV distribution systems', *IEEE Trans. Power Syst.*, 2016, 31, (3), pp. 2192-2203

[17] Zhang, L., Cheng, H., Zhang, S., Zeng, P., Yao, L.: 'Probabilistic power flow calculation using the Johnson system and Sobol's quasi-random numbers', *IET Gener. Transm. Distrib.*, 2016, 10, (12), pp. 3050-3059

[18] Xie, Z. Q., Ji, T. Y., Li, M. S., Wu, Q. H.: 'Quasi-Monte Carlo based probabilistic optimal power flow considering the correlation of wind speeds using copula function', *IEEE Trans. Power Syst.*, 2017

[19] Abdelaziz M. M. A.: 'OpenCL-accelerated probabilistic power for active distribution networks', *IEEE Trans. Sustain. Energy*, 2017

[20] Zhou, G., Bo, R., Chien, L., Zhang, X., Yang, S., Su, D.: 'GPU-accelerated algorithm for online probabilistic power flow', *IEEE Trans. Power Syst.*, 2018, 33, (1), pp. 1132-1135

[21] Martinez-Velasco, J. A., Guerra, G.: 'Reliability analysis of distribution systems with photovoltaic generation using a power flow simulator and a parallel Monte Carlo approach', *Energies*, 2016, 9, (7), pp. 1-21

[22] Hariri, A., Faruque, M. O.: 'A hybrid simulation tool for the study of PV integration impacts on distribution networks', *IEEE Trans. Sustain. Energy*, 2017, 8, (2), pp. 648-657

[23] Baghaee, H. R., Mirsalim, M., Gharehpetian, G. B., Talebi, H. A.: 'Fuzzy unscented transform for uncertainty quantification of correlated wind/PV microgrids: possibilistic-probabilistic power flow based RBFNNs', *IET Gener. Transm. Distrib.*, 2017, 11, (6), pp. 867-877

[24] Peng, S., Tang, J., Li, W.: 'Probabilistic power flow for AC/VSC-MTDC hybrid grids considering rank correlation among diverse uncertainty sources', *IEEE Trans. Power Syst.*, 2017, 32, (5), pp. 4035-4044

[25] Xiao, Q.: 'Dimension reduction method for probabilistic power flow calculation', *IET Gener. Transm. Distrib.*, 2015, 9, (6), pp. 540-549

[26] Tang, J., Ni, F., Ponci, F., Monti, A.: 'Dimension-adaptive sparse grid interpolation for uncertainty quantification in modern power systems: probabilistic power flow', *IEEE Trans. Power Syst.*, 2016, 31, (2), pp. 907-919

[27] Ren, Z., Li, W., Billinton, R., Yan, W., 'Probabilistic power flow analysis based on the stochastic response surface method', *IEEE Trans. Power Syst.*, 2016, 31, (3), pp. 2307-2315

[28] Rouhani, M., Mohammadi, M., Kargarian, A.: 'Parzen window density estimator-based probabilistic power flow with correlated uncertainties', *IEEE Trans. Sustain. Energy*, 2016, 7, (3), pp. 1170-1181

[29] Ni, F. Nguyen, P. H., Cobben J. F. G.: 'Basis-adaptive sparse polynomial chaos expansion for probabilistic power flow', *IEEE Trans. Power Syst.*, 2017, 32, (1), pp. 694-704

[30] Ren, Z., Wang, K., Li, W., Jin, L., Dai, Y.: 'Probabilistic power flow analysis of power systems incorporating tidal current generation', *IEEE Trans. Sustain. Energy*, 2017, 8, (3), pp. 1195-1203

[31] Yin, H., Zivanovic, R.: 'Using probabilistic collocation method for neighbouring wind farms modeling and power flow computation of South Australia', *IET Gener. Transm. Distrib.*, 2017, 11, (14), pp. 3568-3575

[32] Lin, C.-H., Hsieh, W.-L., Chen, C.-S., Hsu, C.-T., Ku, T.-T.: 'Optimization of photovoltaic penetration in distribution systems considering annual duration curve of solar irradiation', *IEEE Trans. Power Syst.*, 2012, 27, (2), pp. 1090-1097

[33] Hung, D. Q., Mithulananthan, N., Lee, K. Y.: 'Determining PV penetration for distribution systems with time-varying load models', *IEEE Trans. Power Syst.*, 2014, 29, (6), pp. 3048-3057

[34] Montoya-Bueno, S., Muñoz, J. I., Contreras, J.: 'A stochastic investment model for renewable generation in distribution systems', *IEEE Trans. Sustain. Energy*, 2015, 6, (4), pp. 1466-1474

[35] Ding, F., Nagarajan, A., Chakraborty, S., Baggu, M., Nguyen, A., Walinga, S., McCarty, M., Bell, F.: 'Photovoltaic impact assessment of smart inverter volt-var control on distribution system conservation voltage reduction and power quality'. *National Renewable Energy Laboratory*, Golden, CO, Tech. rep. NREL/TP-5D00-67296, December 2016

[36] Mather, B.: 'Fast determination of distribution-connected PV impacts using a variable time-step quasi-static time-series approach'. *National Renewable Energy Laboratory*, Golden, CO, Tech. rep. NREL/CP-5D00-67769, August 2017

[37] Deboever, J., Grijalva, S., Reno, M. J., Broderick, R. J.: 'Fast quasi-static time series (QSTS) for yearlong PV impact studies using vector quantization', *Sol. Energy*, 2018, 159, pp. 538-547

[38] Graham, V. A., Hollands, K. G. T.: 'A method to generate synthetic hourly solar radiation globally', *Sol. Energy*, 1990, 44, (6), pp. 333-341

[39] Erbs, D. G., Klein, S. A., Beckman, W. A.: 'Estimation of degree-days and ambient temperature bin data from monthly-average', *ASHRAE Journal*, 1983, 25, pp. 60-65

[40] Short, T. A.: 'Electric Power Distribution Handbook' (*CRC Press* LLC, 2004, Boca Raton, Florida)

[41] Lambert, T., Gilman, P., Lilienthal, P.: 'Micropower system modeling with HOMER', in Farret, F. A., Simões, M. G. (Eds.): 'Integration of Alternative Sources of Energy' (*John Wiley & Sons*, 2006), pp. 379-418

[42] Rampinelli, G. A., Krenzinger, A., Romero, F. C.: 'Mathematical models for efficiency of inverters used in grid connected photovoltaic systems', *Renew. Sust. Energ. Rev.*, 2014, 34, pp. 578-587

[43] Teng, J.-H.: 'A direct approach for distribution system load flow solutions', *IEEE Trans. Power Del.*, 2003, 18, (3), pp. 882-887

[44] Teng, J.-H.: 'Modelling distributed generations in three-phase distribution load flow', *IET Gener. Transm. Distrib.*, 2008, 2, (3), pp. 330-340

[45] Seguin, R., Woyak, J., Costyk, D., Hambrick, J., Mather, B.: 'High-penetration PV integration handbook for distribution engineers'. *National Renewable Energy Laboratory*, Golden, CO, Tech. rep. NREL/TP-5D00-63114, January 2016

[46] Kheldoun, A., Bradai, R., Boukenoui, R., Mellit, A.: 'A new golden section method-based maximum power point tracking algorithm for photovoltaic systems', *Energy Convers. Manage.*, 2016, 111, pp. 125-136

[47] Green, M. A., Emery, K., Hishikawa, Y., Warta, W., Dunlop, E. D.: 'Solar cell efficiency tables (version 47)', *Prog. Photovolt.: Res. Appl.*, 2015, 24, (1), pp. 3-11

[48] Khodr, H. M., Ocque, L., Yusta, J. M., Rosa, M. A.: 'New load flow method S-E oriented for large radial distribution networks'. *Transmission & Distribution Conference and Exposition: Latin America*, Caracas, Venezuela, August 2006, pp. 1-6

[49] Das, D., Kothari, D. P., Kalam, A.: 'Simple and efficient method for load flow solution of radial distribution networks', *Int. J. Elec. Power*, 1995, 17, (5), pp. 335-346